Available online at www.sciencedirect.com
ScienceDirect
Biochimica et Biophysica Acta 1758 (2006) 960–967
BIOCHIMICA ET BIOPHYSICA ACTA
BBA
www.elsevier.com/locate/bbamem

Molecular determination of liver fibrosis by synchrotron infrared microspectroscopy

Kan-Zhi Liu [a,*], Angela Man [a], R. Anthony Shaw [a], Binhua Liang [a], Zhaolin Xu [b], Yuwen Gong [b]

[a] *Institute for Biodiagnostics, National Research Council of Canada, 435 Ellice Ave. Winnipeg, MB, Canada R3B 1Y6*
[b] *The Faculty of Medicine, University of Manitoba, Winnipeg, Canada*

Received 10 January 2006; received in revised form 8 May 2006; accepted 9 May 2006
Available online 17 May 2006

Abstract

Liver fibrosis is an adaptive response to various injuries and may eventually progress to cirrhosis. Although there are several non-invasive methods available to monitor the progression of liver fibrogenesis, they cannot reliably detect fibrosis in its early stages, when the process can be stopped or reversed by removing or eliminating the underlying etiological agent that cause the hepatic injury. In this study, early fibrosis alterations were characterized biochemically, morphologically, and spectroscopically in a rat bile duct ligation (BDL) model. Progressive elevations in serum alanine transaminase (ALT), aspartate transaminase (AST), and bilirubin levels in the BDL rats were found indicating the dynamic deterioration of hepatocellular function. Immunofluorescence microscopy using monoclonal anti-collagen III antibody further revealed abnormal intertwined networks of collagen fibres surrounding the portal areas and extending into the lobules towards the central veins in all BDL samples starting from week one. Synchrotron infrared microspectroscopy of liver sections was exploited to generate false color spectral maps based upon a unique and strong collagen absorption at 1340 cm^{-1}, revealing a collagen distribution that correlated very well with corresponding images provided by immunofluorescence imaging. We therefore suggest that infrared microspectroscopy may provide an additional and sensitive means for the early detection of liver fibrosis.

Keywords: Liver fibrosis; Cirrhosis; Infrared; Mapping; Collagen

1. Introduction

Liver fibrosis and cirrhosis are common sequelae of chronic liver injuries, emerging through wound-healing processes in the liver. Progressive formation of a fibrillar extracellular matrix (ECM) in the liver is the consequence of repeated liver injuries in response to a variety of insults, including chronic viral infection (commonly hepatitis B and C), toxins (e.g., alcohol), and both metabolic and autoimmune disorders [1]. Liver fibrosis results from a dynamic process in which fibrillar ECM formation is associated with ECM degradation and remodelling. This is a balanced process that may either progress to an advanced stage defined as 'cirrhosis' or be reversed to restore normal hepatic structure and function [2]. Cirrhosis is characterized by the formation of regenerative nodules of liver parenchyma that are separated by and encapsulated in fibrotic septa and is associated with major angio-architectural changes. It is generally considered that liver fibrosis is reversible while cirrhosis is irreversible unless an effective treatment for the underlying insult is available.

The need for rapid, safe and reliable methods to detect and monitor the liver fibrogenic progression has become an urgent clinical reality due to increased knowledge regarding the mechanisms responsible for hepatic fibrogenesis and hence the introduction of potentially more effective therapeutic strategies [3]. The concept of a 'fibrosis progression rate' has implications for risk stratification, prognosis and for the evaluation of therapy [4]. Although there has been considerable effort to identify serum markers as non-invasive measures of hepatic fibrosis, e.g., alterations in

* Corresponding author. Tel.: +1 204 984 6476; fax: +1 204 984 5472.
E-mail address: Kan-Zhi.Liu@nrc.ca (K.-Z. Liu).

0005-2736/$ - see front matter © 2006 Elsevier B.V. All rights reserved.
doi:10.1016/j.bbamem.2006.05.006

Table 1
Serum markers for hepatic functions in sham and BDL-treated group

		0 week	2 weeks	4 weeks
ALT	Sham	78.0±3.2	63.0±3.5	61.0±1.0
	BDL-treated	68.6±5.1	176.0±15.1*	165.5±18.6*
AST	Sham	109.6±2.9	98.3±14.9	145.5±44.5
	BDL-treated	112.3±24.1	645.5±126.9*	763.7±97.1*
BIL	Sham	0.5±0.2	0.9±0.3	1.1±0.4
	BDL-treated	0.7±0.3	8.2±1.5*	8.2±1.2*

ALT and AST are in units/liter and bilirubin in mg/dl. The data were obtained from twelve rats for each group and are depicted as Mean±SE.
* indicate significant differences ($P<0.05$).

hepatic TIMP and MMP expression and serum hydroxyproline and hydroxylysine levels, the accuracy and predictive value of these measures are insufficient to provide the basis for clinical decision-making [5,6]. From the clinical standpoint, liver biopsy is still considered the 'gold standard' to confirm the clinical diagnosis, to assess the severity of necro-inflammation and fibrosis, to evaluate possible concomitant disease processes, and to guide therapeutic intervention. However, needle liver biopsy is associated with potential morbidity and mortality and has a high rate of sampling error in patients with diffuse parenchymal liver diseases [7]. For instance, needle liver biopsy sampling error may occur despite an adequate sample size and a satisfactory sampling of portal tracts, when evaluating the severity of inflammation [8], the degree of fibrosis [9], and presence of cirrhosis [7]. The present approach, if successful, might permit routine, accurate, non-subjective diagnostic assessment of very small-bore needle biopsies, minimizing morbidity and at the same time providing clear guidance in the evaluation of treatment options.

While biopsy samples are often stained with either hematoxylin and eosin (H&E) or specific connective tissue stains such as Masson's trichrome or reticulin silver impregnation [10], visualization of fibrosis is not easy and underestimation of the fibrillar ECM network is common [3]. Therefore, most pathologists routinely resort to more specific approaches such as picrosirius red staining [11] or immunofluorescence [12] that provide excellent definition of the distribution of fibrillar collagens (i.e., collagen type I and type III) [13]. These methods clearly reveal the connective tissue structure of liver tissue, including aspects of both perisinusoidal and pericellular fibrosis.

Infrared microspectroscopy offers the means to characterize the nature and distribution of tissue components by virtue of differences among the mid-IR spectra of those components. For example, IR microspectroscopy has been used to demonstrate differences between diseased and normal colon [14], cervical [15], and brain [16] tissues, and changes in composition with apoptosis and necrosis [17]. Of particular relevance here, IR microspectroscopy has been utilized previously to reveal the spatial distribution of collagen (and other components) within both cardiac and oral cancer tissues [18,19]. Collagens exhibit a series of unique IR absorption bands between 1000 and 1350 cm^{-1}, and these have been exploited in previous studies characterizing collagen tissue distribution [18–23]. For instance, an absorption at 1204 cm^{-1} was used as a marker band to characterize collagen distribution in heart tissue and oral cancers [18,19], while a band at 1338 cm^{-1} was shown to be directly related to the quantity of collagen in cartilage and exploited for a study of prostatic hyperplasia [21,22]. Liver tissue has been characterised by infrared microspectroscopy in two previous studies [23,24].

The spatial resolution of conventional infrared microspectroscopy is limited by diminishing signal-to-noise with small apertures. Therefore, fine tissue architectural features cannot be resolved with regular infrared microspectroscopy. Fortunately, this problem can be alleviated by employing synchrotron infrared radiation as a source, since it is 1000 times brighter than a standard black-body source. As a result, spectra with good signal-to-noise may be acquired with apertures at or near the diffraction limit [25,26]. By utilizing a synchrotron IR source, it is possible to resolve tissue architectural features at a spatial resolution near the diffraction limit (~10 μm at 1000 cm^{-1}), and to reveal structures that would not otherwise be resolved by conventional IR microspectroscopy.

Therefore, in the current study, we made use of synchrotron infrared microspectroscopy (at the National Synchrotron Light Source) to examine the distribution of liver fibrosis within a rat model, and compared the resulting maps to images produced from the same tissue section by immunofluorescence staining (monoclonal anti-collagen III antibody).

2. Material and methods

2.1. Animal model

A total of twenty-four adult male Sprague–Dawley rats were obtained from the Animal Facility of the University of Manitoba. All rats were maintained under 12-h light/dark cycles with food and water ad libitum. All animals received humane care in compliance with criteria set by the Canadian Council on Animal Care. These rats were divided into two groups, sham-operated and bile duct ligation (BDL), respectively. Since the BDL model represents the major features of liver fibrosis with significant modification of ECM and has been used most frequently for the investigation of liver fibrosis, we implemented this model according to a procedure described previously [27–30]. Briefly, the animal was subjected to mild anesthesia and the common bile duct was exposed by median laparotomy and occluded by double ligature with a nonresorbable suture (7-0 silk). The first tie was made below the junction of the hepatic ducts and the second was made above the entrance of the pancreatic duct. The common bile duct was then resected between the two ligatures, and the abdominal incision was closed. Liver specimens were then collected weekly (4 animals weekly; 24 animals total), up to 6 weeks following BDL by excision of the entire liver. These specimens were frozen in liquid nitrogen immediately following removal, and stored at −70 °C for further analysis.

2.2. Serum and liver biochemistry

Blood samples were obtained from the saphenous vein of rats at 0, 2, and 4 weeks intervals after sham or BDL procedures. The serum concentrations of alanine transaminase (ALT) and aspartate transaminase (AST) were determined using a Roche-Hitachi 917 Clinical Chemistry Analyzer with Roche application kit while bilirubin levels were measured using a bilirubin assay kit from Sigma (Sigma-Aldrich Inc, St. Louis, USA).

2.3. Liver histology

Frozen liver samples (approx. 0.5 cm^3) were randomly taken from the right, median and left lobes of each rat liver and sectioned consecutively at 5 μm using a cryostat at −18 °C. These sections were mounted on slides and air dried for at least 20 min followed by fixation in 10% Formalin for 30 s. Then these sections were stained with routine Haematoxylin and Eosin according to regular staining procedure such as hydration, staining, dehydration and clearing. The stained slides were finally covered with a cover-slip using a mounting medium Entellen.

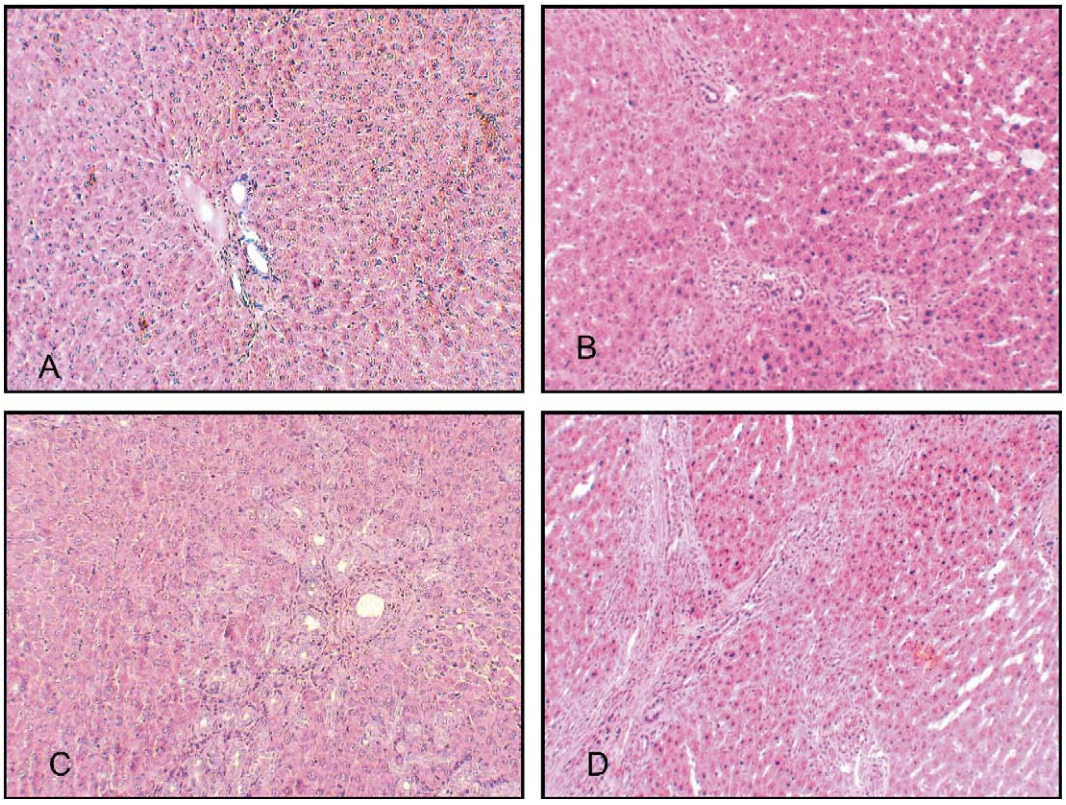

Fig. 1. Representative liver tissues stained with hematoxylin and eosin (×100 magnification). A: SHAM group (4 weeks); B: BDL group (1 week); C: BDL group (2 weeks); D: BDL group (4 weeks).

2.4. Immunofluorescence histochemistry

Frozen, unfixed liver samples were embedded in optimal temperature cutting (OCT) compound, sectioned consecutively at 10 μm in a cryostat at −18 °C and mounted on 25 mm barium fluoride windows. These windows permitted both immunofluorescence staining and infrared microspectroscopic imaging (regular glass slides are opaque to mid-IR radiation). The tissue sections were then fixed in pre-cooled 100% acetone (− 20 °C) for 10 min, washed twice with PBS, then incubated with Alexa Fluor 488 (Molecular Probes, Eugene, USA) conjugated monoclonal anti-collagen III antibody (Sigma-Aldrich Inc, St. Louis, USA) in a humid chamber at 37 °C for 60 min in the dark. This monoclonal anti-collagen III antibody is produced in mouse and the species reactivity are human and rat. The concentration of the antibody was 1:625. The windows were then washed three times with PBS and mounted with coverslips using fluorescent mounting medium (DAKO Diagnostics Canada, Inc, Mississauga, Canada). Negative controls were treated with omission of the monoclonal anti-collagen III antibody on adjacent sections cut from the same tissue sample. These sections were examined using an inverted Nikon Eclipse TS100 microscope equipped with Nikon Plan Fluor objectives (Nikon, Tokyo, Japan), a Fluor filter set (Omega Optical, Brattleboro, USA) and a 300 W Xenon light source (Intracellular Imaging Inc, Cincinnati, USA). Microfluorographic images were captured as monochrome digital signals by a Cohu 2600 series CCD camera (Cohu, Inc., Electronics Division, San Diego, USA) coupled to the microscope. The fluorescence intensities were calibrated with the InSpeck Microscope Image Intensity Calibration Kits (Molecular Probes, Eugene, USA) to keep the experimental conditions constant for each experiment. The fluorescence images in Fig. 2 were generated from this fluorescence imaging system.

2.5. IR microspectroscopy

Infrared spectra of liver tissue sections were collected using a FTIR microscope attached to a Nicolet Magna 860 spectrometer that receives its source light from Beamline U2B at the National Synchrotron Light Source, Brookhaven National Laboratory, Upton, NY [31]. Specifically, liver sections stained with Alexa Fluor 488 conjugated monoclonal anti-collagen III antibody were mounted on IR transparent BaF_2 windows and placed in position for mid-IR microspectroscopic measurements. A video camera mounted to the microscope captured visible images before data collection. Prior to spectral data collection, fluorescence images were obtained, using an Olympus BX-FLA fluorescence accessory mounted to the IR microscope [32] with a specific filter set (excitation: 460–500 nm; dichroic: 505 nm; emission: 510–540 nm; Chroma Technology Corp., Brattleboro, VT). These permitted precise registration of features within the IR microspectroscopy images with their fluorescence counterparts.

An adjustable aperture was placed before the objective to limit the IR illumination area to a 10 by 10 μm pixel, calibrated using a visible light image at its focal point. For each pixel, a spectrum was acquired using 64 coadditions and Happ-Genzel apodization at 4 cm^{-1} resolution. Prior to data collection, a background spectrum through air (no sample) was collected as a reference so data could be converted to absorbance. The spectral data were acquired using Atlus software (Thermo Nicolet Instruments Corporation). FTIR spectra for each pixel within the IR map were first smoothed using the Savitsky–Golay algorithm, followed by the application of a second derivative operation within the microspectroscopy imaging software (CytoSpec; www.cytospec.com) employed to generate IR images.

2.6. Statistical analysis

ANOVA was used to analyze differences in serum marker levels for the sham vs. BDL groups. Differences with P values below 0.05 were deemed to be significant.

3. Results

In the current study, early fibrosis was investigated in a rat bile duct ligation model using morphological and spectroscopic methods. Analysis of plasma enzymes carried out in parallel

revealed progressive elevations in serum alanine transaminase (ALT), aspartate transaminase (AST) and bilirubin levels which usually suggest the dynamic deterioration of hepatocellular function, and are indicative of cholestatic liver disease [33–35]. A 2.5-fold increase in ALT and a 6.5-fold increase in AST were observed after the first 2 weeks of bile duct ligation, and the activities of these two enzymes remained elevated throughout the experimental period (Table 1). Similar results were also observed for bilirubin.

Routine H&E staining was employed to characterize representative liver sections from sham and BDL groups at various timepoints following BDL occlusion, as displayed in Fig. 1. The liver tissue from sham group (Fig. 1A) showed a portal track (portal triad) in the middle with its bile ductule and hepatic arterial and portal venous branches. The hepatocytes had normal histological appearance, i.e., they were polyhedral with eosinophilic cytoplasm and a usually central nucleus. Between the cords of hepatocytes are endothelially lined sinusoids. Neither inflammatory cell infiltration nor portal or periportal fibrosis was found. However, for the BDL group, mild bile duct proliferation was evident in the portal tract after the first week and progressively exacerbated thereafter, associated with some mild inflammatory cell infiltrate around the ducts and portal vessels (Fig. 1B–D). Specifically, after 2 weeks of BDL, the typical ductular reaction associated with progressive deposition of extracellular matrix surrounding the newly formed bile ducts became obvious (Fig. 1C). At the fourth week of BDL, the alteration of liver structure was even more evident, with bridging fibrosis encircling most of the newly formed bile ducts (Fig. 1D).

To further confirm the early stage of fibrosis in this BDL model, and to create a molecular image of collagen deposition and distribution for comparison with the IR maps, we carried out immunofluorescence staining of the liver section with Alexa Fluor 488 conjugated monoclonal anti-collagen III antibody (Fig. 2). As expected, in the sham tissue, only blood vessels and bile ducts (both of which are rich in collagen) are visible while the hepatocytes, lymphocytes, Kupffer, and sinusoidal endothelial cells are invisible in the dark field (Fig. 2A). However, in the BDL model, newly formed bile ducts were readily detected by fluorescence staining; some deposition of fibrous tissue was observed as early as the first week following BDL (Fig. 2B). After 2 weeks of BDL, newly formed bile ducts progressively invaded the other parts of the lobule and were surrounded by fibrous tissue (Fig. 2C). By the fourth week post-BDL, an intense fluorescent network was evident, revealing extensive interweaved and threaded fibrils within the liver tissue ECM (Fig. 2D).

Prior to processing and interpretation of the IR microspectroscopic liver tissue spectra, we compared the spectrum of calf type III collagen (Sigma-Aldrich Inc, St. Louis, USA) to that of normal liver tissues to characterize the basic spectroscopic differences between normal hepatocytes and collagenous tissue (Fig. 3). The IR spectrum of liver tissue showed the absorptions typical of tissue

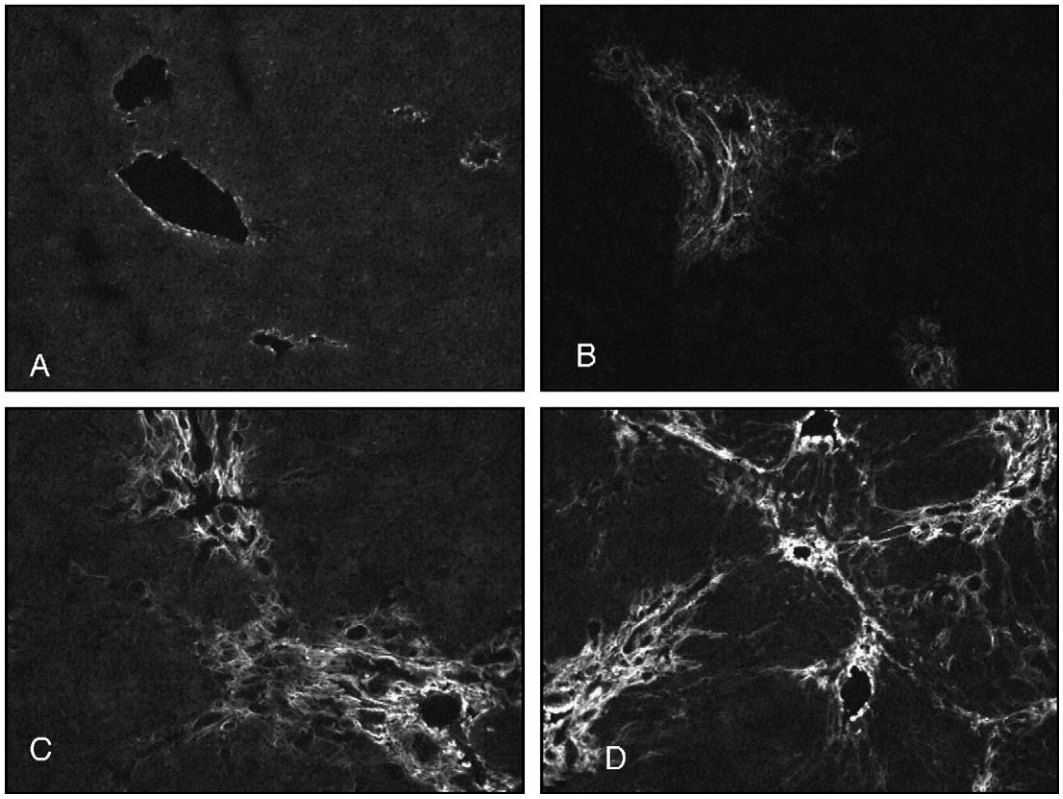

Fig. 2. Representative liver tissues immunofluorescence-stained with Alexa Fluor 488 conjugated monoclonal anti-collagen III antibody (×100 magnification). A: SHAM group (4 weeks); B: BDL group (1 week); C: BDL group (2 weeks); D: BDL group (4 weeks).

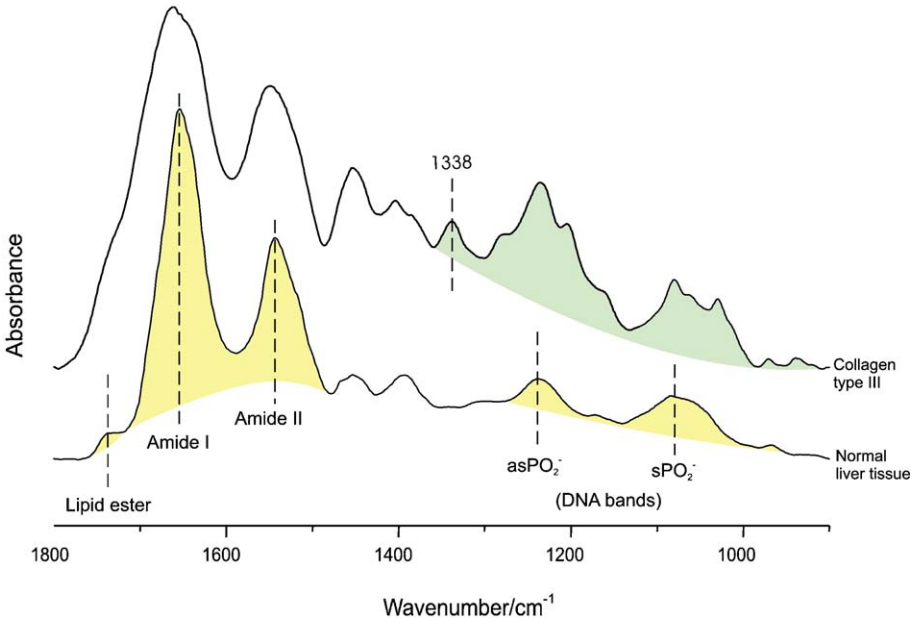

Fig. 3. Infrared spectra for normal liver tissue and pure type III collagen.

proteins, lipids (membranes) and nucleic acids. For instance, the two prominent absorptions at 1652 cm^{-1} and 1542 cm^{-1} arise from C═O stretching (amide I) and N–H bending (amide II) vibrations of the protein peptide groups [36]. The bands marked as sPO_2^- and $asPO_2^-$, located at 1087 and 1240 cm^{-1}, are the symmetric and asymmetric PO_2^- stretching vibrations of the DNA phosphodiester

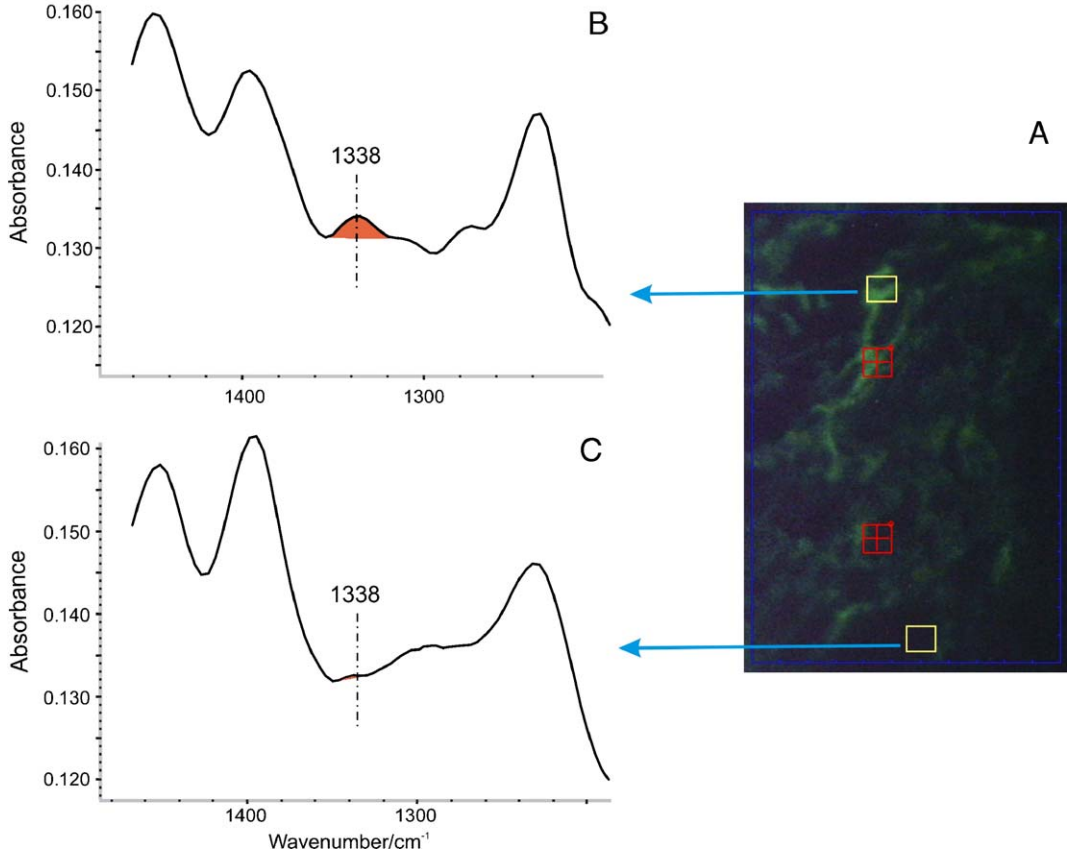

Fig. 4. Section from 1-week post-BDL liver tissue stained with immunofluorescence monoclonal anti-collagen III antibody (A). Comparison of infrared spectra obtained from pixels coincident with representative fibrotic (B) and normal (C) liver.

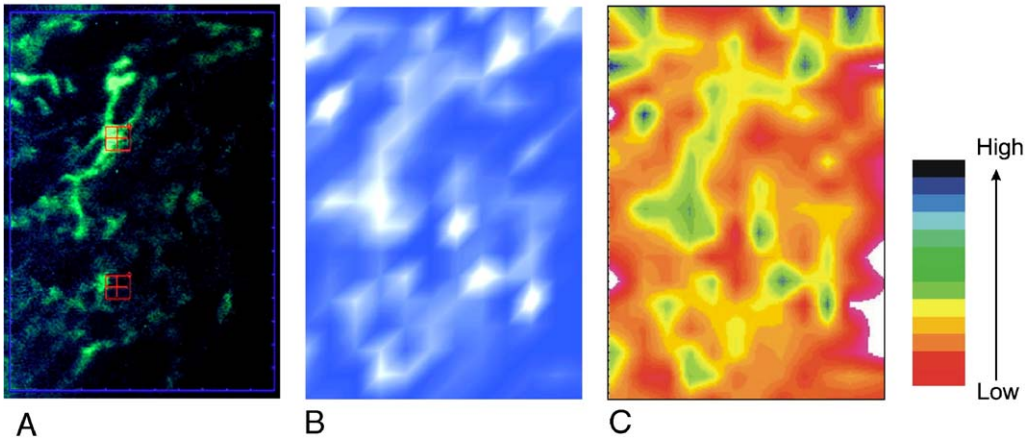

Fig. 5. Collagen distribution images. Immunofluorescence-stained (1-week BDL) liver tissue section image (A) is compared to the corresponding digital image (B) and two-dimensional contour map (C) derived from the 1338 cm^{-1} collagen absorption within the infrared microspectroscopic map for the same tissue section.

groups (with the protein amide III band also contributing intensity at 1240 cm^{-1}), and lipids contributed a band centered at 1740 cm^{-1} that originates from the ester C═O group.

The major spectral features distinguishing collagen and liver tissue are the collagen absorptions between 1000 and 1350 cm^{-1} arising from vibrations of the collagen sidechains, predominantly from the proline groups. A number of infrared absorptions which are highly characteristic of collagen have been identified previously, and used as IR markers of collagen deposition in the heart and other tissues [18–20,37]. Here, we have chosen to use the marker band at 1338 cm^{-1}, since other collagen absorptions in this region overlap heavily with DNA bands in the liver tissue (Fig. 3). To confirm that this dominant collagen band can indeed be used for the detection of liver fibrosis, we extracted absorption spectra representative of a high fluorescence area (collagen-rich) and a low fluorescence area as shown in Fig. 4. As expected, the band at 1338 cm^{-1} is significantly stronger within the fibrotic, collagen-enriched area as compared to normal liver, as demonstrated in Fig. 4B and C. The collagen band at 1338 cm^{-1} was therefore adopted as the basis to map collagen deposition for detection and characterization of liver fibrosis.

To investigate the overall collagen deposition within the liver sections from BDL rats, immunofluorescence staining with Alexa Fluor 488 conjugated monoclonal anti-collagen III antibody was used as a gold standard to reveal the subtle fibrosis in a liver section after 1 week of BDL (Fig. 5A). A grid of IR spectra was also obtained from the same area by raster-scanning synchrotron IR microspectroscopy, to provide the basis to generate IR maps. Imaging software (CytoSpec) was then used to import these spectral data and produce false color images generated from the intensity of the 1338 cm^{-1} collagen band. As shown in Fig. 5B and C, an IR false color image and two-dimensional contour map accurately recover the distribution of collagen deposition in the liver section, as revealed by the collagen-specific immunofluorescence photomicrograph (Fig. 5A). Moreover, while the IR false color map mimics the collagen distribution pattern as revealed qualitatively by the immunofluorescence photomicrograph, the two dimensional contour map goes further, permitting quantification of the collagen deposition in the same section (Fig. 5B and C).

4. Discussion

Common bile duct ligation and scission in rats, as used in this study, represents a classical experimental model for the analysis of the events from the initial injury of the bile ducts through the organization of a fibrotic reaction [25,38]. The combination of raised intra-biliary pressure, release of inflammatory mediators, anoxia, and the cytotoxic effect of bile acids induce inflammatory processes leading to hepatic fibrosis and finally to secondary biliary cirrhosis [39]. The major advantages of this model are the significant infiltration of the connective tissues in the portal zone and enhanced proliferation of bile duct epithelial cells and hepatocytes; therefore, it is often used to understand ECM expression and its regulation during the cholestasis, and hepatocyte proliferating activity in the fibrosis process [39].

The BDL model was successfully established in the current study, as reflected by the morphologic changes within the liver sections and by the associated serum biochemical alterations reflecting deteriorated liver function (Fig. 1 and Table 1), in agreement with previous studies [38–41]. Immunofluorescence imaging of these BDL liver sections further revealed the structural changes characteristic of this model, including disordered liver architecture with bile duct proliferation and fibrous deposition in the intracellular matrix (Fig. 2). Moreover, these pathological changes were observed to be time dependent; by the fourth week of BDL, severe collagen deposition was observed in the intracellular matrix, including significant infiltration of connective tissue in the portal zone and progressive accumulation of newly formed bile ducts. Therefore, this model – in conjunction with immunofluorescence imaging – can be reliably employed to evaluate the feasibility and accuracy of IR mapping for the early detection of liver fibrosis, as executed in the current protocol.

It is well documented that the visualization of fibrosis in the liver specimen is not always easy with routine H&E staining or with Masson's trichrome, which can underestimate the extension of fibrosis [3]. The adaptation of more specific methods on a routine basis is therefore considered crucial. These alternative methods include picrosirius red staining [11] which provides an excellent characterization of the distribution of fibrillar collagens

(i.e., collagen type I and type III), or reticulin staining that allows a reasonable analysis of the connective tissue structure of liver tissue, including features of pericellular and perisinusoidal fibrosis [13]. Other methods such as immunohistochemistry for proteins typical of fibrillar ECM (e.g., pro-collagen type I, III, and VI, tenascin, etc.) have also proposed, although these remain at the experimental stage [42]. Immunofluorescence staining was the best choice for the current protocol since it can reveal specific collagen types (e.g., type III) while not interfering with IR measurements. Therefore, simultaneous determination of collagen deposition in the tissue was possible by both IR microspectroscopy and immunofluorescence staining within the same area of interest from same slide with excellent registration (Fig. 5).

It is well known that the ECM of liver is composed of several molecular forms of collagen (predominantly types I, III and IV) and noncollagenous components such as undulin, elastin, fibronectin, and laminin [43]. With liver fibrosis, the total content of collagens and noncollageneous components increases, accompanied by a shift of ECM from a low-density basement membrane-like matrix (e.g., type IV) to an interstitial type matrix containing fibril-forming collagens (type I, III) [44]. It has also been suggested that collagen type III and fibronectin accumulate in the early liver injury whereas collagen I, IV, undulin, elastin and laminin predominate in the chronic or late stage [44,45]. Thus, the employment of type III collagen antibody is appropriate for the current study, focussed on detection and characterization of the early stages of liver fibrosis (Fig. 2).

Because the fibrillar network is so diffuse and filamentous in nature, IR microspectroscopy at lower spatial resolution would be incapable of resolving the structures so clearly revealed by the fluorescence image of Fig. 5A. The dominant advantage of synchrotron microspectroscopy is illustrated well by the images of Fig. 5B and C, which do faithfully reproduce the general features revealed by immunofluorescence staining. It is also important to point out, however, that the representative IR image does not perfectly match the corresponding fluorescence stained image. The discrepancies may originate from any of several sources. Most likely, we believe, is the specificity of the collagen stain. Although the most dominant collagen in the early stage of liver fibrosis is type III, other collagens such as collagen type I and fibronectin are also implicated in the alteration of liver ECM. While the immunofluorescence image would not reflect these collagens, IR microspectroscopy would. A second source of discrepancy may be the fact that the spatial resolution of IR microspectroscopy is lower than that of the fluorescence imaging technique. The resolution of synchrotron IR microspectroscopy (10 μm in the mid-infrared region) [46] does not match the resolution of the immunofluorescence image, which is on the order of 0.5 μm [47]. Therefore, it is not surprising to see that the images generated by immunofluorescence and IR imaging techniques are not perfect matches.

In summary, IR microspectroscopy can detect liver fibrosis with its own unique "false color imaging" approach to reveal the subtle and early fibrosis within the ECM. IR microspectroscopy possesses numerous potential advantages over traditional approaches to regular pathology. For instance, fixation and staining of tissues are not required before histological viewing. Secondly, since the IR spectrum simultaneously samples numerous molecular species, it is capable (for example) of detecting various collagen types associated with fibrosis, e.g., collagen I, III, IV and fibronectin, without resorting to separate antibodies as required by immunofluorescence or other histopathologic methods. Furthermore, additional biochemical information (e.g., DNA, RNA, glycogen, lipids content) is available simultaneously from same spectroscopic dataset, as exploited in previous spectroscopic liver studies [23,24]; this feature can provide additional information regarding the severity of fibrosis. Further studies will focus on the use of IR digital staining to quantify liver fibrosis from very small samples (e.g., needle biopsies) both for the routine confirmation of clinical diagnosis and to guide therapeutic intervention.

Acknowledgements

This study was kindly supported by the Manitoba Medical Service Foundation and The National Synchrotron Light Source, Brookhaven National Laboratory, Upton, New York, USA. We sincerely appreciate the hospitality and assistance from Dr. Lisa Miller in carrying out the synchrotron microspectroscopy measurements at NSLS.

References

[1] S.L. Friedman, Alcoholic liver disease, cirrhosis, and its major sequelae, in: L. Goldman, J.C. Bennett (Eds.), Cecil Textbook of Medicine, 21th ed., W.B.Saunders, Philadelphia, 2000, pp. 804–812.
[2] S.L. Friedman, Liver fibrosis—From bench to bedside, J. Hepatol. 38 (2003) S38–S53.
[3] M. Pinzani, K. Rombouts, S. Colagrande, Fibrosis in chronic liver diseases: diagnosis and management, J. Hepatol. 42 (2005) S22–S36.
[4] J.D. Collier, T. Woodall, D.G. Wight, S. Shore, A.E. Gimson, G.J. Alexander, Predicting progressive hepatic fibrosis stage on subsequent liver biopsy in chronic hepatitis C virus infection, J. Viral Hepatitis 12 (2005) 74–80.
[5] R. Lichtinghagen, D. Michels, C.I. Haberkorn, B. Arndt, M. Bahr, P. Flemming, M.P. Manns, K.H. Boeker, Matrix metalloproteinase (MMP)-2, MMP-7 and tissue inhibitor of metalloproteinase-1 are closely related to the fibroproliferative process in the liver during chronic hepatitis C, J. Hepatol. 34 (2001) 239–247.
[6] E.J. Kucharz, Serum hydroxyproline and hydroxylysine levels in patients with decompensated cirrhosis, Rom. J. Internal Med. 32 (1994) 271–274.
[7] J. Poniachik, D.E. Bernstein, K.R. Reddy, et al., The role of laparoscopy in the diagnosis of cirrhosis, Gastrointest. Endosc. 43 (1996) 568–571.
[8] P. Schlichting, B. Holund, H. Poulsen, Liver biopsy in chronic aggressive hepatitis. Diagnostic reproducibility in relation to size of specimen, Scand. J. Gastroenterol. 18 (1983) 27–32.
[9] L.J. Jeffers, A. Findor, S.N. Thung, et al., Minimizing sampling error with laparoscopic guided liver biopsy of right and left lobes, Gastrointest. Endosc. 37 (1991) 266.
[10] G.S. Montes, Structural biology of the fibres of the collagenous and elastic systems, Cell Biol. Int. 20 (1996) 15–27.
[11] L.C. Junqueira, W. Cossermelli, R. Brentani, Differential staining of collagens type I, II and III by Sirius Red and polarization microscopy, Arch. Histol. Jpn. 41 (1978) 267–274.
[12] J. Friemann, B. Voss, W. Weller, K.M. Muller, Asbestos induced fibrosis in the omentum of rats. Immunofluorescence microscopical demonstration of collagens types I and III; laminin and fibronectin, Virchows Arch. A Pathol. Anat. Histopathol. 411 (1987) 403–408.
[13] H. Puchtler, F.W. Waldrop, Silver impregnation methods for reticulum fibers and reticulin: a re-investigation of their origins and specificity, Histochemistry 57 (1978) 177–187.
[14] P. Lasch, W. Haensch, D. Naumann, M. Diem, Imaging of colorectal adenocarcinoma using FT-IR microspectroscopy and cluster analysis, Biochim. Biophys. Acta 1688 (2004) 176–186.

[15] M.J. Romeo, M.A. Quinn, F.R. Burden, D. McNaughton, Influence of benign cellular changes in diagnosis of cervical cancer using IR microspectroscopy, Biopolymers 67 (2002) 362–366.
[16] G. Steiner, R.A. Shaw, L.-P. Choo-Smith, M.H. Abuid, G. Schackert, S. Sobottka, W. Steller, R. Salzer, H.H. Mantsch, Distinguishing and grading human gliomas by IR spectroscopy, Biopolymers 72 (2003) 464–471.
[17] N. Jamin, L. Miller, J. Moncuit, W.H. Fridman, P. Dumas, J.L. Teillaud, Chemical heterogeneity in cell death: combined synchrotron IR and fluorescence microscopy studies of single apoptotic and necrotic cells, Biopolymers 72 (2003) 366–373.
[18] K.Z. Liu, I.M. Dixon, H.H. Mantsch, Distribution of collagen deposition in cardiomyopathic hamster hearts determined by in microscopy, Cardiovasc. Pathol. 8 (1999) 41–47.
[19] C.P. Schultz, K.Z. Liu, P.D. Kerr, H.H. Mantsch, In-situ infrared histopathology of keratinization in human oral/or pharyngeal aqueous cell carcinoma, Oncol. Res. 10 (1998) 277–286.
[20] M. Jackson, L.P. Choo, P.H. Watson, W.C. Halliday, H.H. Mantsch, Beware of connective tissue proteins: assignment and implications of collagen absorptions in infrared spectra of human tissues, Biochim. Biophys. Acta 1270 (1995) 1–6.
[21] M.J. Li, H.S. Hsu, R.C. Liang, S.Y. Lin, Infrared microspectroscopic detection of epithelial and stromal growth in the human benign prostatic hyperplasia, Ultrastruct. Pathol. 26 (2002) 365–370.
[22] N.P. Camacho, P. West, P.A. Torzilli, R. Mendelsohn, FTIR microscopic imaging of collagen and proteoglycan in bovine cartilage, Biopolymers 62 (2001) 1–8.
[23] M. Diem, L. Chiriboga, H. Yee, Infrared spectroscopy of human cells and tissue. VIII. Strategies for analysis of infrared tissue mapping data and applications to liver tissue, Biopolymers 57 (2000) 282–290.
[24] L. Chiriboga, H. Yee, M. Diem, Infrared spectroscopy of human cells and tissue. Pert VI: a comparative study of histopathology and infrared microspectroscopy of normal, cirrhotic, and cancerous liver tissue, Appl. Spectrosc. 54 (2000) 1–8.
[25] N. Jamin, P. Dumas, J. Moncuit, W.H. Fridman, J.L. Teillaud, G.L. Carr, G.P. Williams, Chemical imaging of nucleic acids, proteins and lipids of a single living cell. Application of synchrotron infrared microspectrometry in cell biology, Cell. Mol. Biol. 44 (1998) 9–13.
[26] L.M. Miller, J. Tibrewala, C.S. Carlson, Examination of bone chemical composition in osteoporosis using fluorescence-assisted infrared microspectroscopy, Cell. Mol. Biol. 46 (2000) 1035–1044.
[27] D. Jalink, F.J. Urbanski, S.S. Lee, Bilioenteric anastomosis reverses hyperkinetic circulation in bile duct-ligated cirrhotic rats, J. Hepatol. 25 (1996) 924–931.
[28] C.C. Chan, C.C. Chang, H.C. Huang, S.S. Wang, F.Y. Lee, et al., Effects of norepinephrine and acetylcholine on portal-systemic collaterals of common bile duct-ligated cirrhotic rat, J. Gastroenterol. Hepatol. 20 (2005) 1867–1872.
[29] N.M. Atucha, F.J. Nadal, A. Alcaraz, D. Iyu, M.C. Ortiz, J. Garcia-Estan, Reduced capacitative calcium entry in the mesenteric vascular bed of bile duct-ligated rats, Eur. J. Pharmacol. 525 (2005) 117–122.
[30] R. Rodrigo, R. Jover, A. Candela, A. Compan, J. Saez-Valero, S. Erceg, V. Felipo, Bile duct ligation plus hyperammonemia in rats reproduces the alterations in the modulation of soluble guanylate cyclase by nitric oxide in brain of cirrhotic patients, Neuroscience 130 (2005) 435–443.
[31] L.M. Miller, G.L. Carr, M. Jackson, P. Dumas, G.P. Williams, The impact of infrared synchrotron radiation in biology: Past, present and future, Synchrotron Radiat. News 13 (2000) 31–37.
[32] T. Tague, L.M. Miller, Development of an infrared microscope with fluorescence capabilities, Microsc. Today 2 (2000) 26–32.
[33] M. Weinreb, R.D. Pollak, Z. Ackerman, Experimental cholestatic liver disease through bile-duct ligation in rats results in skeletal fragility and impaired osteoblastogenesis, J. Hepatol. 40 (2004) 385–390.
[34] V. Shah, S. Cao, H. Hendrickson, J. Yao, Z.S. Katusic, Regulation of hepatic eNOS by caveolin and calmodulin after bile duct ligation in rats, Am. J. Physiol.: Gasterointest. Liver Physiol. 280 (2001) G1209–G1216.
[35] H. Ji, J.Y. Jiang, Z. Xu, E.A. Kroeger, S.S. Lee, H. Liu, H. Shen, M. Zhang, G.Y. Minuk, P.C. Choy, Y. Gong, Change in lipid profile and impairment of endothelium-dependent relaxation of blood vessels in rats after bile duct ligation, Life Sci. 73 (2003) 1253–1263.
[36] W.K. Surewicz, H.H. Mantsch, D. Chapman, Determination of protein secondary structure by Fourier transform infrared spectroscopy: a critical assessment, Biochemistry 32 (1993) 389–394.
[37] K.Z. Liu, M. Jackson, M.G. Sowa, H. Ju, I.M.C. Dixon, H.H. Mantsch, Modification of the extracellular matrix following myocardial infarction monitored by FTIR spectroscopy, Biochim. Biophys. Acta 1315 (1996) 73–77.
[38] J. Kountouras, B.H. Billing, P.J. Scheuer, Prolonged bile duct obstruction: A new experimental model of cirrhosis in the rat, Br. J. Exp. Pathol. 65 (1984) 305–311.
[39] J. Wu, P.A. Norton, Animal models of liver fibrosis, Scand. J. Gastroenterol. 31 (1996) 1137–1143.
[40] F. Marra, R. DeFranco, G. Robino, E. Novo, E. Efsen, S. Pastacaldi, E. Zamara, A. Vercelli, B. Lottini, C. Spirli, M. Strazzabosco, M. Pinzani, M. Parola, Thiazolidinedione treatment inhibits bile duct proliferation and fibrosis in a rat model of chronic cholestasis, World J. Gastroenterol. 11 (2005) 4931–4938.
[41] L. Beljaars, K. Poelstr, G. Molema, D.K.F. Meijer, Targeting of sugar- and charge-modified albumins to fibrotic rat livers: the accessibility of hepatic cells after chronic bile duct ligation, J. Hepatol. 29 (1998) 579–588.
[42] H.P. Dinges, K. Zatloukal, H. Denk, J. Smolle, S. Mair, Alcoholic liver disease. Parenchyma to stroma relationship in fibrosis and cirrhosis as revealed by three-dimensional reconstruction and immunohistochemistry, Am. J. Pathol. 141 (1992) 69–83.
[43] M. Rojkind, M.A. Giambrone, L. Biempica, Collagen types in normal and cirrhotic liver, Gastroenterology 76 (1979) 710–719.
[44] L. Galligani, M. Lonati Galligani, G. Fuller, Collagen metabolism in the liver of normal and carbon tetrachloride treated rats, Biomedicine 31 (1979) 199–200.
[45] A.D. Burt, M.R. Griffith, D. Schuppan, B. Voss, R.N. MacSween, Ultrastructural localization of extracellular matrix proteins in liver biopsies using ultracryomicrotomy and immuno-gold labelling, Histopathology 16 (1990) 53–58.
[46] N. Jamin, P. Dumas, J. Moncuit, W.H. Fridman, J.L. Teillaud, G.L. Carr, G.P. Williams, Highly resolved chemical imaging of living cells by using synchrotron infrared microspectrometry, Proc. Natl. Acad. Sci. U. S. A. 95 (1998) 4837–4840.
[47] B. Bailey, D.L. Farkas, D.L. Taylor, F. Lanni, Enhancement of axial resolution in fluorescence microscopy by standing-wave excitation, Nature 366 (1993) 44–48.